Structure-Based Identification of the Binding Site for the Hemiasterlin Analogue HTI-286 on Tubulin

Malini Ravi,*,‡ Arie Zask,‡ and Thomas S. Rush III§

Chemical and Screening Sciences, Wyeth Research, 401 North Middletown Road, Pearl River, New York 10965, and Chemical and Screening Sciences, Wyeth Research, 87 Cambridge Park Drive, Cambridge, Massachusetts 02140

Received July 1, 2005; Revised Manuscript Received August 24, 2005

ABSTRACT: A binding mode of HTI-286, a synthetic analogue of the peptidic antimitotic agent hemiasterlin, to tubulin is proposed. The binding mode was derived from iterative docking experiments directed at regions of the tubulin interdimer interface that are believed to be consistent with all current experimental data regarding the HTI-286/tubulin interaction. These data include (1) competitive inhibition of the tubulin binding of the Vinca alkaloids and other antimitotic agents, (2) proximity to stretches of amino acid residues identified in two separate photoaffinity-labeling experiments, (3) structure−activity relationships for HTI-286 and its analogues, (4) saturation transfer difference nuclear magnetic resonance (NMR) experiments, and (5) NMR transfer nuclear Overhauser effect spectroscopy (NOESY) experiments that potentially identify the bioactive conformation. The predicted binding mode thus affords a means to understand the mode of action of hemiasterlin, HTI-286, and other closely related molecules.

Small molecule tubulin-binding agents have been a major focus of chemotherapeutic drug development efforts for the treatment of cancer (*1*−*7*). The cytotoxic activity of such agents arises from their ability to interfere with the functions of the mitotic spindle by disrupting the dynamic equilibrium of microtubules (*1*, *6*, *8*). The complex dynamics of microtubules consists of varying rates of growth and dissociation and is regulated by the presence of guanosine 5′-triphosphate (GTP).[1] Because the biological functions of microtubules are dependent upon their polymerization dynamics, anti-microtubule agents can inhibit cell proliferation and thus be used as therapeutic agents in the treatment of various forms of cancer. Owing to their importance in mitosis and cell division, microtubules are considered by some as representing the best cancer target to be identified thus far (*4*). Further, with the number of new cancer cases exceeding 10 million as well as the large number of cancer-related deaths worldwide (*9*), the development of anticancer therapy is brought to the forefront of research.

Antimicrotubule agents are chemically diverse, consisting of compounds that are categorized by their ability to act either as stabilizers or destabilizers of microtubule formation. The taxanes, which include Taxol and Taxotere, are found to stabilize microtubule formation. The microtubule-destabilizing Vinca alkaloids are the earliest tubulin-binding antimitotics to be used in the clinic (*6*). Although there is little direct structural evidence, destabilizing antimitotics are believed to alter the topology of protofilament formation by altering the contacts between tubulin subunits (*10*, *11*). Further, it is surmised that some conformational change in the tubulin component of the protein−ligand complex may be involved in effecting the disruption of microtubule dynamics (*10*).

Several experimental studies probing the binding of mitotic inhibitors to tubulin have appeared in the literature (*11*−*14*). However, the complexity and diversity of tubulin−ligand binding compounded with the lack of corroborating structural evidence have served as inherent limitations to an understanding of the detailed molecular interactions present in the system under study. To bridge the gap to a molecular level understanding, experimental data are often used to help drive computational studies aimed at predicting the binding modes of antimitotic agents. An excellent example is found in a recent publication of Nettles et al. (*12*), where the tubulin-binding mode of epothilone, a microtubule stabilizer, is obtained through the supportive use of electron crystallography. Rai and Wolff have localized the binding region of the microtubule-destabilizing agent vinblastine to be contained within residues 175−213 of β tubulin (*15*). Dolastatin-10, hemiasterlin, and Cryptophycin-52, three peptides that are competitive inhibitors of each other but noncompetitive inhibitors of the Vinca alkaloids, have been studied by various experimental and computational methods (*11*, *16*, *17*).

A significant amount of experimental data has recently been accumulated on the interaction of tubulin with HTI-286. A synthetic analogue of the naturally occurring tripeptide hemiasterlin, HTI-286, has demonstrated biological activity in preclinical cancer models (*18*). Biophysical

* To whom correspondence should be addressed. E-mail: ravim@wyeth.com. Telephone: (845) 602-8085. Fax: (845) 602-5561.

‡ Chemical and Screening Sciences, Wyeth Research, Pearl River, NY.

§ Chemical and Screening Sciences, Wyeth Research, Cambridge, MA.

[1] Abbreviations: GDP, guanosine 5′-diphosphate; GTP, guanosine 5′-triphosphate; NOE, nuclear Overhauser effect; NOESY, nuclear Overhauser effect spectroscopy; TRNOESY, transferred nuclear Overhauser spectroscopy; STD, saturation transfer difference; rmsd, root-mean-square deviation; SAR, structure−activity relationship.

10.1021/bi051268b CCC: $30.25
Published on Web 11/10/2005

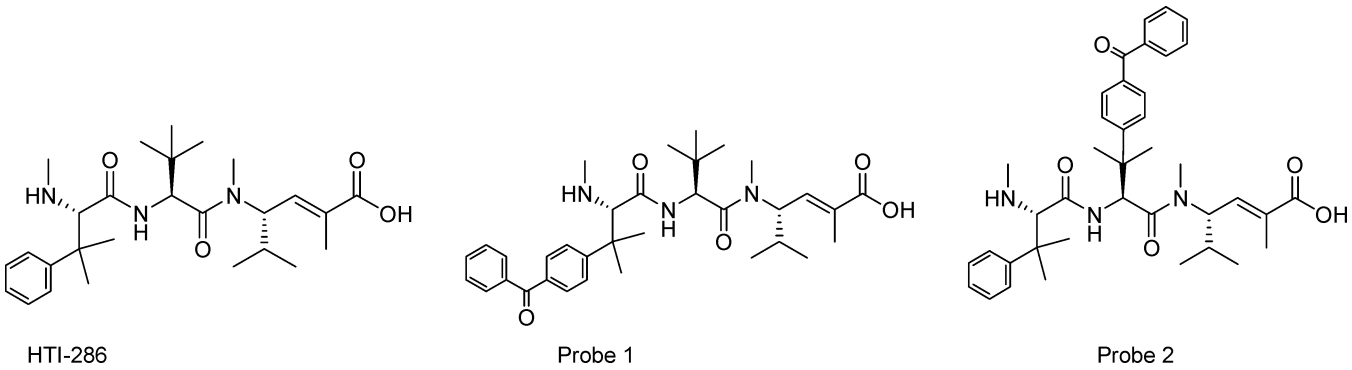

FIGURE 1: Chemical structures of HTI-286 and the two photoaffinity probe analogues.

characterization experiments of Krishnamurthy et al. (*19*) confirm that the observed antimitotic activity is a result of the binding interactions between tubulin and HTI-286. Sedimentation equilibrium analyses were used to show that HTI-286 binds the tubulin heterodimer and oligomerizes it to a 13-unit ring structure. Localization of the HTI-286 binding site on the tubulin heterodimer was also facilitated by the work of Nunes et al. (*20*), where photoaffinity analogues of HTI-286 were used to define cross-linking sites involving regions of α tubulin proximal to the interdimer interface. On the basis of competitive binding studies with dolastatin-10, cryptophycin A, vinblastine, paclitaxel, and colchicines, Nunes et al. have hypothesized that the hemiasterlin analogues interact with the *β*-tubulin subunit within the area carved out as the binding region of the Vinca alkaloids (residues 175−213) such that cross-linking of two photoaffinity probes to α tubulin is facilitated. In addition, two separate nuclear magnetic resonance (NMR) studies of HTI-286 and its photoaffinity probe analogues by Milton et al. at Wyeth Research, which will be published in a separate paper, have helped to gain a more detailed understanding of the interactions of tubulin with the respective ligands. These studies include saturation transfer NMR experiments to probe protein−ligand interactions and nuclear Overhauser effect spectroscopy (NOESY) experiments to probe the bound conformation of the ligand. Last, the structure−activity relationship (SAR) data of Zask et al. (*21*−*24*) uncover various aspects of tubulin binding to HTI-286 and its analogues.

The present computational study of HTI-286 aims at proposing a putative binding mode that is cumulatively supported by the experimental data from biophysical characterization, photolabeling studies, and NMR studies, as well as biological activity data. An understanding of the tubulin−inhibitor interactions at the molecular level is afforded by these structure-based studies in which the electron crystallographic (3.5 Å resolution) structure of Löwe et al. served as the 3D protein structure (*25*). Given the low resolution of the protein structure, an iterative docking procedure, which was consistent with available SAR, was used to direct as well as fine-tune the computational model. Of particular significance is that the proposed protein−ligand interaction scheme is well-correlated with an extensive SAR for hemiasterlin analogues resulting from the synthetic efforts of Zask et al., as well as with both of the photoaffinity probe cross-linking regions mapped out by Nunes et al. Furthermore, bound conformations of HTI-286 and its photoaffinity analogues are in good agreement with the findings of the NMR investigations of Milton et al., regarding ligand conformation and protein−ligand contacts.

MATERIALS AND METHODS

Receptor Model. The initial receptor model employed in these studies was built from the 3.5 Å resolution electron crystallography-derived structure of the α/*β*-tubulin dimer of Löwe et al. The crystallographic symmetry group ($P12_1$) and unit cell dimensions $a = 81.2$ and $b = 93.5$ of the structure (*25*) were used to create an α/*β*−α/*β* tetramer, because the experimental evidence points to a binding region proximal to the interdimer interface. The Accelrys software package, Quanta, (*26*) was used to perform this task. The complex is oriented such that the C terminus of the α-tubulin subunit of one dimer is adjacent to the N terminus of the *β*-tubulin subunit of the second dimer, as also described by Nogales et al. (*27*). After the four-unit tubulin complex was constructed, we removed the outer two subunits to help reduce computational time, leaving only the central *β*−α tubulin dimer. The interdimer interface, which is the focus of this study, consists of the C terminus of the α-tubulin unit and the N terminus of the *β*-tubulin unit.

Ligand Models. The 3D structures of HTI-286 and two photoaffinity probes, probe 1 and probe 2 (shown in Figure 1), were first built and minimized using the molecular modeling package Sybyl and its implementation of the MMFF94 force field (*28*). The molecules were then conformationally expanded using the OpenEye Scientific Software package, Omega (*29*), with an 8 kcal maximum and a 1.0 Å root-mean-square deviation (rmsd) cutoff to filter out degenerate conformers.

Molecular Docking and Scoring. Overall, our docking and scoring procedure involved extensive rigid-body sampling with a commercial docking program, dynamics and minimization runs of the top-ranked poses output from this program, and a final scoring step with a solvent-based scoring function. For the initial binding pose sampling, we chose to use the OpenEye Scientific Software package FRED (*30*). Briefly, FRED exhaustively searches a predefined docking site/box and scores and filters each binding pose with respect to a shape-based (Gaussian) and a final user-specified scoring function. In this study, we chose to sample poses derived from both Gaussian/PLP and Gaussian/ChemScore scoring schemes. In general, PLP consists of a steric matching function with a less stringent charge matching function (*31*), while ChemScore consists of more detailed matching criteria for lipophilic and electrostatic aspects of protein−ligand

interactions (*32*). The top 10 poses for each ligand at each putative binding site were then passed along for further evaluation.

The FRED-based sampling was performed in and around the interdimer interface in eight discrete areas to save computational time. All eight areas fit the available experimental data such that they all would place the ligands in the vicinity of the alleged Vinca-binding domain and place the probes in or around the protein segments to which they covalently bind.

The best protein−ligand complexes from the FRED sampling procedure were then optimized using a dynamics-based scheme before they were scored with the final scoring function and analyzed with respect to the available SAR. Here, a 5 Å region including the ligand and nearby protein residues was optimized by iteratively running molecular dynamics simulations followed by energy minimizations of selected low-energy frames from the dynamics trajectory carried out at 300 K for 10 ps at a step size of 10 fs. This procedure was carried out in Sybyl6.9 with the MMFF94s force field.

Finally, each relaxed receptor−ligand complex was scored with a more rigorous Poisson Boltzmann/Molecular Mechanics-based (PBMM-SA) scoring function (*33*). Here, the free energy of protein−ligand binding is described (scored) as

$$\Delta G_{\mathrm{bind}}^{\mathrm{solv}} = \Delta G_{\mathrm{bind}}^{\mathrm{gas}} - \Delta G_{\mathrm{solv}}^{\mathrm{P}} - \Delta G_{\mathrm{solv}}^{\mathrm{L}} + \Delta G_{\mathrm{solv}}^{\mathrm{PL}}$$

where the first term to the right of the equal sign is the gas-phase protein−ligand binding energy and is obtained via molecular mechanics calculations. The remainder of the terms represent the solvated free-energy terms for the protein and ligand individually as well as the protein−ligand complex. The solvated free-energy terms are evaluated explicitly via Poisson Boltzmann/surface area calculations (*33*). Solvation as well as hydrophobic effects are aptly handled by this scoring function, while they are not in either the PLP or ChemScore scoring functions. The best scoring modes were then assessed for their ability to explain the existing SAR.

RESULTS

Our tiered docking procedure quickly led us to a pocket in the β subunit that is proximal to the interdimer interface and places HTI-286 and the probes within "striking distance" of the photoaffinity-labeled amino acid stretches of both the α and β subunits. This area (shown in Figure 2) accommodates very well the peptide-like nature of the ligand and allows sufficient burial of hydrophobic portions of the molecule. The majority of the best scoring poses for each ligand was found here. The residues that make up this binding pocket include Ser174, Ser178, and Asp179 of β tubulin and Phe351 of α tubulin.

Nonetheless, the last step in our procedure was to take all of the best scoring poses after the PBMM-SA scoring step and assess their ability to explain the existing NMR and SAR, the two pieces of experimental data not yet used to drive the binding pose prediction. This aspect of the pose selection is described in detail in the Discussion.

The final binding mode chosen to represent the tubulin−HTI-286 complex is shown in Figures 2 and 3. This binding

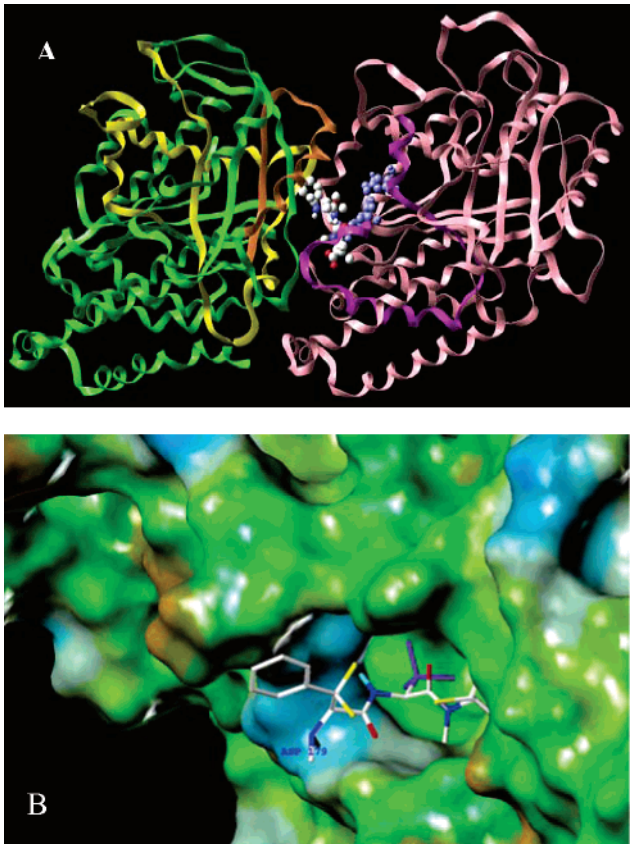

FIGURE 2: Best HTI-286 binding pose and its interactions with tubulin. (A) Overview of the α/β-tubulin complex used in the docking studies and the best binding pose for HTI-286, emphasizing the proximity to the photoaffinity regions. The Vinca-binding region (175−213) of the β subunit is colored purple, and the remaining region of β tubulin is colored pink. The photoaffinity cross-linking regions of probes 1 and 2 are colored orange and yellow, respectively, and the remaining region of α tubulin is colored green. HTI-286 and GDP are shown in CPK representation, where GDP is colored blue, while HTI-286 is colored by atom type. (B) Surface view of HTI-286 docked to the β-tubulin portion of the interdimer interface, emphasizing the binding pocket. The α-tubulin subunit is not shown for clarity. The tubulin surface is colored by lipophilic potential (brown, hydrophobic; green, neutral; and blue, hydrophilic). Hydrogens are removed for simplicity. The yellow-colored carbon atoms are poised for intramolecular interactions, and the *tert*-butyl carbons are colored purple.

mode (a) scores well for all ligands, (b) is in agreement with competition data, (c) places the reactive moiety of the photoaffinity groups next to the stretches of amino acids labeled in the experiments of Nunes et al. (Figure 4), (d) is in agreement with saturation transfer difference (STD) NMR experiments, (e) places the ligand in a 3D conformation consistent with NMR experiments, and (f) explains the available SAR. Overall, this pose appears to be driven by favorable van der Waals interactions and the hydrophobic effect, while favorable electrostatic interactions are mostly balanced by desolvation costs. The relative magnitudes of each of the contributions to the PBMM-SA score are shown in Table 1. Details of the molecular level interactions are presented below.

The binding scores afford a means of assigning relative ranks to bound poses. The data presented in Table 1 are largely similar for all three analogues, as expected on the basis of the similarity in the corresponding binding modes. The additional benzophenone moiety of the probe analogues

FIGURE 3: Stick view of HTI-286 bound to tubulin. Interactions with key residues of β tubulin, as discussed in the text, are shown. Key hydrogen bonds are indicated with a dashed yellow line. Intramolecular interactions found in the bound conformation are apparent. The residues of the photoaffinity cross-linking regions of probes 1 and 2 are colored orange and yellow, respectively. The carbon atoms of residues belonging to the Vinca-binding region are colored purple.

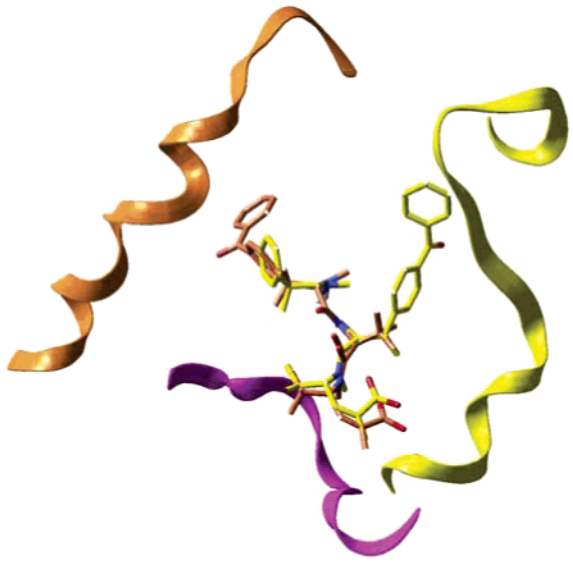

FIGURE 4: Bound conformation of HTI-286 with the photoaffinity probes. The structure of probe 2 is overlayed onto the structure of probe 1. The Vinca-binding region of the β subunit is colored purple. The photoaffinity cross-linking regions as well as the carbon atoms of probes 1 and 2 are colored orange and yellow, respectively.

Table 1: Computed Energy Scores for HTI-286 and Probe Analogues

structure	total score	electrostatic score (coulomb + solvation)	hydrophobic score	van der Waals score
HTI-286	−37.1	13.8	−8.9	−42.0
probe 1	−37.4	15.2	−9.6	−43.0
probe 2	−38.5	14.9	−9.9	−43.5

is reflected in the slightly more favorable van der Waals and hydrophobic scores as well as in the higher desolvation costs apparent in the electrostatic score. In summary, more favorable van der Waals and hydrophobic scores offset the desolvation cost, resulting in total binding scores that are comparable to the scores computed for protein−ligand complexes with biological activities in the low micro- to nanomolar range. Rush et al. compare several protein−ligand systems scored in this manner (33).

Finally, the optimized protein−ligand complex consists of an optimal orientation of the ligand within a favorable binding region created by the relocation of local protein residues in response to the molecular dynamics simulations and optimizations. To ensure that we did not artificially create a favorable binding pocket during the flexible part of our procedure, we evaluated the cost of creating the ligand-binding pocket within the β subunit. To do so, we performed a Powell minimization using the MMFF94 force field within Sybyl of a 5.0 Å spherical region around the binding site, with and without the ligand present, and then compared the energy difference. In each case, the computed internal energies for the 5 Å region of the tubulin complex were favorable toward binding. Further, as detailed below, the conformational changes in the ligand-binding region are consistent with the curvature at the α/β interdimer interface.

DISCUSSION

In the end, our best scoring binding mode agreed quite well with all experimental data, although the calculations were only driven by the facts that these molecules bind in the Vinca-binding region and label within specific stretches of tubulin amino acids in the photoaffinity experiments. We were quite pleased to find that the best scoring mode agreed with the additional NMR data and our own SAR for HTI-286 analogues, although this information was not used during the docking procedure.

According to our predictions, there are several important factors contributing to the HTI-286/tubulin interaction. These include several contact/hydrophobic interactions, hydrogen bonding, and electrostatic complementarity. Overall, the cumulative set of protein−ligand interactions define the U-shaped curvature of the backbone of HTI-286. The tertiary butyl group is found to occupy a spacious cavity in β tubulin, proximal to the location of the guanosine 5′-diphosphate (GDP), the E-site nucleotide, in the 3D representation of the tubulin dimer used in this study. The 5-position *N*-methyl group is found to interact with alkyl side chains of nearby residues. Similarly, favorable interactions of the 2-position methyl group with nearby alkyl chains are apparent. The binding model finds the C-1 position of HTI-286 to be oriented in a region of β tubulin that is flanked by two ASN residues (residues 186 and 101 of the β-tubulin subunit) providing hydrogen-bonding opportunities with the carbonyl or hydroxyl group of the ligand. The interaction of the NH at the C-10 position with the side chain of Asp179 is consistent in each of the optimized views of the modeled tubulin−HTI-286 complex. Average distances of 3.0−3.5 Å are observed between the NH and the Asp179 side chain. The heteroatoms of the amide backbone of HTI-286 are seen forming β-sheet-like interactions with the backbone atoms of nearby amino acid residues. The C-6 carbonyl group is found within approximately 3.0 Å of the side chain of Ser178 in the β-tubulin unit. The 8-postion NH moiety is found within approximately 2.5 Å of Ser178 in the β-tubulin unit. In the two interactions described above, we find that probe 2 favors a closer association with Ser174, while probe 1 favors Ser178.

Perhaps most significant is the agreement of the binding model with the experimental data from the explorations of

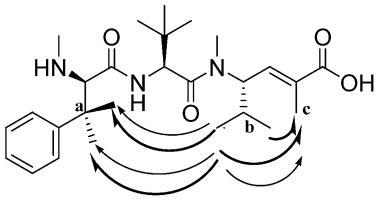

FIGURE 5: Details of HTI-286 intramolecular interactions. A comparison of predictions from modeling studies with those of NMR studies.

the tubulin-binding site using the HTI-286 photoaffinity probes. (Also important is that all 3 models coincide!) On the basis of peptide-mapping studies, the cross-linking region of probe 1, is within residues 314−339 of the α-tubulin subunit. In comparison, the binding model of this probe places the reactive carbonyl moiety within close proximity to Ile332 of the α-tubulin subunit. In addition to the aforementioned scaffold interactions with tubulin, it also appears that favorable π-stacking interactions between the phenyl ring of HTI-286 and the side chain of Phe351 of α tubulin are formed. A similar binding orientation is found for probe 2, where the reactive benzophenone group is attached to the *tert*-butyl moiety of HTI-286. Studies on probe 2 resulted in the favorable π-stacking interaction of the phenyl ring of the benzophenone group and the side chain of Tyr224 of the β-tubulin unit. The close approach of the carbonyl moiety of probe 2 to Leu248 of the α-tubulin unit is consistent with photoaffinity data, indicating the cross-linking region to include residues 204−280 of α tubulin.

Further support of our binding model is afforded by the transferred nuclear Overhauser spectroscopy (TRNOESY) NMR studies of Milton et al., our colleagues at Wyeth Research. In their study, they found that the bound conformation of HTI-286 and the photoaffinity analogues display intramolecular nuclear Overhauser effect (NOE) interactions between the C-11 geminal dimethyl group and one of the methyl groups attached to C-4. The same intramolecular orientations are also seen in the bound conformation of HTI-286 and its probe analogues in these studies. In the binding model proposed here, the methyl group at the C-2 position is found to be nearly equidistant to both methyl groups attached to C-4. The binding model suggests a nearly equidistant orientation of both methyl groups at the C-4 position with a slight preference for one over the other. The data from Milton et al. indicate that there is a greater preference for the interaction of the methyl group at the C-2 position with the same methyl group attached at the C-4 that is found to form NOE interactions with the methyl groups of the C-11 position. The differences between the NMR TRNOESY data and the current study can be summarized as shown in Figure 5. Excellent agreement with three of four intramolecular orientations is seen. The fourth interaction, as depicted by the computational studies, is less discriminating than the corresponding interaction prescribed by the NMR studies in that both methyl groups of atom "b" are poised nearly equidistant with the methyl group at "c". Thus, on the basis of computational studies, it appears that both methyl groups at location "b" can form favorable interactions with methyl group "c".

Milton et al. also carried out saturation transfer NMR studies in an effort to identify portions of the ligand that most closely interact with the protein. These studies involved systems in which combinations of tubulin with HTI-286, probe 1, and probe 2 were probed for interactions between various ligand moieties and protein. The findings of these NMR experiments also support our models. First, they found 70−100% saturation transfer for the aromatic portion of HTI-286. This supports the π-stacking interactions apparent in the binding model between the phenyl ring attached to C-11 of the HTI-286 scaffold and Phe351 of α tubulin. As well, the close approach of the benzophenone moiety of probe 2 to Leu248 of α tubulin results in favorable π-stacking interactions between a phenyl ring of this moiety and Tyr224 of α tubulin. In addition, the very low transfer (∼16−22%) found for the *tert*-butyl group is consistent with the placement of this group in a spacious cavity within β tubulin.

Final support for our binding mode prediction comes from an extensive set of SAR data of HTI-286 and its analogues. The key features of the available SAR are summarized in Figure 6, with sample compounds and biological activities shown in Table 2 (*21*). Compounds were evaluated for their ability to inhibit extracellular tubulin polymerization and for their cytotoxicity in paclitaxel-sensitive KB-3-1 cells and in paclitaxel-resistant KB-8-5 and KB-V1 cells expressing moderate and high levels of P-glycoprotein, respectively. Most importantly, the model supports the significance of a basic moiety at the C-10 position, the role of the tertiary butyl moiety in the binding event, β-sheet-like interactions between the protein and the ligand, the relevance of the type and size of substituents at the N-5 and C-2 positions, and the groups tolerated at the C-1 position.

The importance of the C-10 basic nitrogen for inhibitory activity is well-represented in the binding model. The results of these studies indicate that interactions between the basic NH group of HTI-286 and the Asp179 residue of the β-tubulin subunit are quite significant and that deleting this interaction can have serious consequences to enthalpic and desolvation contributions to binding.

Very little interaction of the *tert*-butyl moiety with the protein is seen, in agreement with the SAR data, indicating that large groups are tolerated at this position. The requirement for branching of the C-7 substituent of the central amino acid is consistent with the reduction of conformational space accessible to the central portion of the peptide by bulkier substituents (*34*). This rigidity pre-organizes the molecule into a conformation necessary for tubulin binding. The need for the *S* configuration and the loss of potency of the analogue with an *R* configuration substantiate the importance of the *tert*-butyl group in binding.

The binding model places the 8-postion NH moiety within 2.5 Å of Ser178 and Asp179 in the β-tubulin unit. In support of this placement, SAR data indicate that N-methylation of the 8-postion NH or removal of the amide carbonyl oxygens leads to analogues with a loss of potency. The binding model indicates an association between Ser174 and Ser178 of the β tubulin and the C-9, C-6, and N-8 positions of the HTI-286 scaffold. The work of Poruchynsky et al. (*35*), in support, finds cells grown in the presence of HTI-286 develop resistance to it and have a Ser174 to Ala174 mutation that results in a 8−20-fold decrease in HTI-286 potency.

The positioning of the N-methyl group of the N-5 position proximal to the alkyl side chains is consistent with the weaker activity of the corresponding NH analogue, favorable ori-

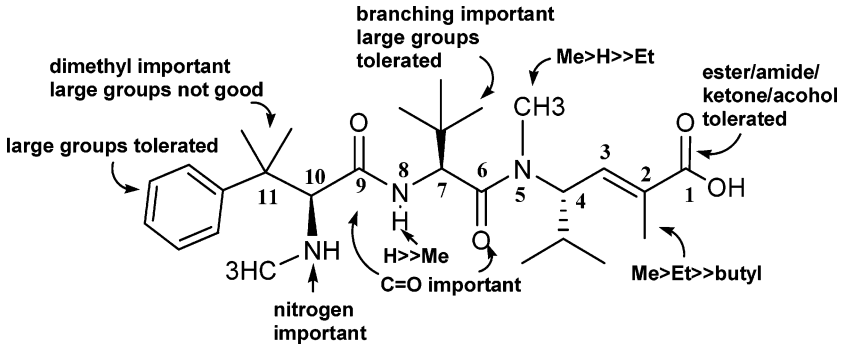

FIGURE 6: Key features of SAR for HTI-286.

Table 2: Summary of Key Features of SAR for Select Compounds with Associated Biological Activity

Compound	Tubulin[a]	KB-3-1[b]	KB-8-5[b]	kb-V1[b]
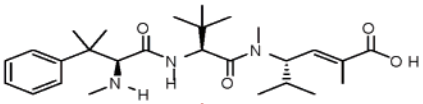	88	0.96	2.3	77.4
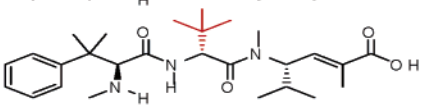	1	>3000	>3000	>3000
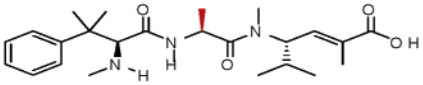	8	381	902	>3000
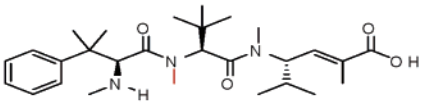	4	>3000	>3000	>3000
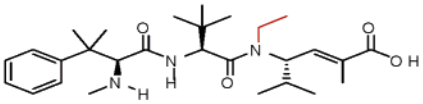	11	109	197	>3000
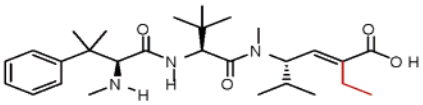	83	5.4	14	513
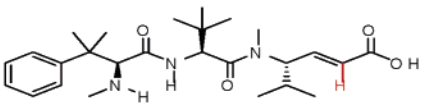	53	191	479	>3000
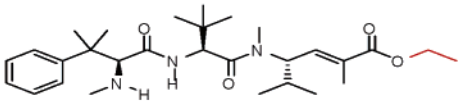	97	34	499	1870
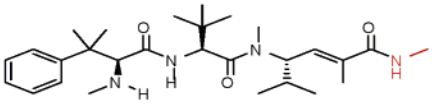	78	68	129	1590

[a] Percent inhibition of tubulin polymerization at 0.3 μM. [b] IC_{50} (in nanomolars) in cells.

entations of the methyl group with nearby alkyl chains are observed. A loss of potency is seen in analogues with hydrophobic substituents larger than the methyl group here, in accordance with the binding model, which affords limited space here. Similarly, the favorable interactions of the 2-position methyl group with nearby alkyl chains are limited in space such that it would be difficult to accommodate larger hydrophobic groups. The SAR supports this because both the analogue without the methyl group as well as analogues with larger groups are less potent.

With regard to the carboxylic group at the 1 position, amides, esters, ketones, and alcohols are tolerated to varying degrees. The placement of this portion of the ligand in the vicinity of two ASN residues is consistent with this.

A comparison of the tubulin-bound conformation of HTI-286 to a minimized unbound conformation is shown in Figure 7. The carbon atoms of the bound and unbound conformations are colored white and green, respectively. We find that, upon binding, the phenyl and geminal dimethyl moieties at the C-11 position reorient to form their respective interactions. This appears to be a key conformational change that allows for favorable interactions with aromatic rings of tubulin residues as well as favorable intramolecular interactions. The role of the basic moiety at C-10 and the *tert*-

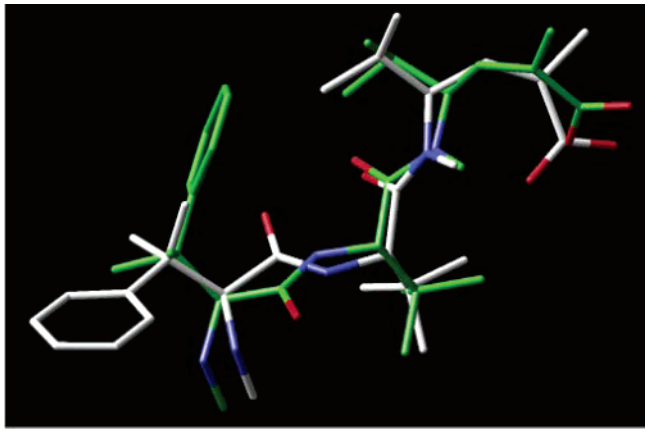

FIGURE 7: Overlay of two HTI-286 conformations. The carbon atoms of the protein-bound conformation and a low-energy conformation are colored white and green, respectively.

butyl moiety at C-7 in tubulin binding appears to be further supported by the reorientation at the N8 and C9 positions such that interactions with nearby residues can be pursued by these moieties. Last, slight conformation changes near the acid moiety enable the close association with ASN residues of β tubulin. In comparison, the tubulin-hemiasterlin binding mode proposed by Mitra et al. (*16*) places the ligand in a similar region of β tubulin proximal to the GDP. Additionally, it appears that the Mitra model favors an overall U-shaped conformation of the hemiasterlin backbone with the tertiary butyl moiety at the apex of the "U", thus sharing some similarity with our proposed model. Further details of interactions of specific portions of hemiasterlin with specific residues of β tubulin are not immediately apparent in the Mitra et al. model. However, the binding orientation of hemiasterlin proposed by Mitra et al. is fundamentally different from the binding orientation of its analogue, HTI-286, proposed here. Contrary to the Mitra model and in strong support of available SAR, our model places the basic amino moiety that is common to both structures in close association with Asp179 (Asp177 in the Mitra et al. model). Further, we place the tertiary butyl moiety in a spacious region adjacent to the GDP and oriented such that a photoaffinity probe attached to the moiety is seen to approach the region of α tubulin (residues 203−280) that is experimentally determined to be the cross-linking region for the probe. In contrast, it appears that the Mitra et al. model would orient a photoaffinity probe attached to the tertiary butyl group, analogous to the probe 2 structure, away from the experimentally determined cross-linking region. Although the α−β interdimer interface was not explicitly modeled in the study by Mitra et al., the photoaffinity data of Nunes et al. (*20*) detailing the cross-linking of probe 1 to residues of the α-tubulin subunit were cited as being consistent with their binding model for hemiasterlin. Mitra et al. also site the proximity of the helix H10 of α tubulin to the bound hemiasterlin as a possible cause of unfavorable steric contacts, which are then alleviated through conformational adjustments resulting in curvature at the interdimer interface. The Mitra et al. model does not include residues of the H10 helix in the binding pocket detailed for hemiasterlin because the α-tubulin unit was not included in the docking study itself. However, we see a significant interaction of the HTI-286 analogues with residues of helix H10 of α tubulin. The benzophenone moiety of probe 1 is found in close proximity to Ile332 of the H10 helix. As well, π-stacking interactions with Phe351 of the adjacent S9 region are significant in our model.

Finally, we would like to discuss results from our binding study that are in support of the idea that ligand-binding effects change to longitudinal contacts at the interdimer interface. First, interactions between aromatic moieties of the protein and ligand are prominent. Domains of the tubulin protein stabilized by aromatic stacking, when modified by factors such as ligand binding, have been linked to microtubule depolymerization (*25*). In the binding model proposed here, the interaction of the HTI-286 aromatic ring with that of Phe351 of the α-tubulin subunit is seen to perturb interactions between Phe351, Phe343, Phe296, and Tyr312 corresponding to the H9, S8, and S9 regions of α tubulin, regions proximal to the interdimer interface. We find that, upon ligand binding, the H10 helix, which is adjacent to strand S9, is oriented closer to the α subunit and farther away from the β subunit of the interdimer interface. On a similar note, the Barbier et al. model of a nine-membered αβ dimer tubulin ring constructed using X-ray data on a curved interdimer interface (*11*) proposes interactions between each of the two phenyl rings of Cryptophycin-52 with the aromatic rings of Tyr208, Phe212, and Tyr222 of β tubulin. Second, we see distancing of key residues of the helix H8 and strand S9 from their positions in the uncomplexed α tubulin. Correia and Lobert suggest that α-Glu254 enjoys close association with the phosphate moieties of GTP in the noncurved interdimer interface, whereas curvature in the interface may cause a displacement of α-Glu254 with respect to the nucleotide resulting in the associated lack of GTPase activity (*10*). Löwe et al. report that α-Glu254 is in direct contact with the nucleotide (*25*). The tubulin−HTI-286 complex modeled in this study indicates a distancing of α-Glu254 from the β phosphate of GDP as compared to the uncomplexed structure of Löwe et al. Thus, the closest approach between the nucleotide and the α-Glu254 side chain in the ligand-bound structure is within 5.8−6.4 Å, whereas this distance is approximately 4.5 Å in the uncomplexed structure. Further, the side chains of α-Lys352 and α-Glu254 are found to be within 1.5 Å in the ligand-bound complex. In comparison, the uncomplexed structure places the two residues at a distance of 3.0 Å. Our results are in support of the suggestion that a distancing of α-Glu254 and the nucleotide occurs at the ligand-bound interdimer interface. We find that, in the ligand-bound complex, the H8 helix of α is found in close contact with β tubulin, while the H10 helix of α tubulin and the H6 helix of β tubulin are found farther apart, rendering curvature to the interdimer interface. In our study, the superposition of the ligand-complexed structure and the uncomplexed structure results in an average rmsd of 1.57 Å for the C_αs. In comparison, Gigant et al. (*36*) report that in their X-ray structure of a tubulin−stathmin-like domain complex, a relative measure of the observed curvature is given in the superposition of the nucleotide-binding domains, where the C_αs are found to have a rmsd of 1.4 Å.

CONCLUSION

Understanding the association of tubulin with antimitotic agents at the molecular level is crucial to future drug

development efforts. However, the pursuit of a molecular level understanding of tubulin−drug binding has been challenging. For example, speculated bioactive conformations of Taxol favoring intramolecular interactions were contradicted by electron crystallographically determined by bound conformations favoring protein−ligand interactions (*12*). The present study proposes a molecular level picture of the interaction between tubulin and HTI-286. Protein−ligand complementary interactions are found to be significant in our binding model. Consistent with binding models for Taxol and Cryptophycin-52, our assessment of tubulin−HTI-286 binding reveals significant π-stacking interactions between protein and ligand aromatic moieties. Similar protein−ligand interactions are also cited in studies where 3D pharmacophore models of drug candidates used as scaffolds around which a shell of amino acids is built and optimized to fit evolving SAR data (*14*). The binding model is in agreement with protein-mapping experiments for two photoaffinity probe analogues. The intramolecular as well as intermolecular contacts made by the bound conformation of the ligand are substantiated with NMR data. In addition, the conformational changes apparent near the tubulin−HTI-286-binding region, as determined by the changes in select inter-residue distances, are consistent with hypothesized modifications in longitudinal contacts, resulting in tubulin ring formation. Overall, there is a need for more extensive structural information on tubulin of higher resolution. However, we present a binding model here that is substantiated by significant experimental data.

ACKNOWLEDGMENT

We thank Semi Ayral-Kaloustian and Frank Loganzo for critical reading of the manuscript and beneficial comments and Lee Greenberger for useful discussions.

REFERENCES

1. Jordan, M. A. (2002) Mechanism of action of antitumor drugs that interact with microtubules and tubulin, *Curr. Med. Chem.: Anti-Cancer Agents 2*, 1−17.
2. Checchi, P. M., et al. (2003) Microtubule-interacting drugs for cancer treatment, *Trends Pharmacol. Sci. 24*, 361−365
3. Goodin, S., Kane, M. P., and Rubin, E. H. (2004) Epothilones: Mechanism of action and biologic activity, *J. Clin. Oncol.: Biology of Neoplasia 22*, 2015−2025.
4. Jordan, M. A., and Wilson, L. (2004) Microtubules as a target for anticancer drugs, *Nat. Rev. Cancer 4*, 253−265.
5. Jordan, A., and Hadfield, J. (1998) Tubulin as a target for anticancer drugs: Agents which interact with the mitotic spindle, *Med. Res. Rev. 18*, 259−296.
6. Dumontet, C., and Sikic, B. (1999) Mechanisms of action of and resistance to antitubulin agents: Mictrotubule dynamics, drug transport, and cell death, *J. Clin. Oncol. 17*, 1061−1070.
7. Altmann, K.-H. (2001) Microtubule stabilizing agents: A growing class of important anticancer drugs, *Curr. Opin. Chem. Biol. 5*, 424−431.
8. Horwitz, S. B. (1992) Mechanism of action of taxol, *Trends Pharmacol. Sci. 13*, 134−136.
9. Mathers, C., Shibaya, K., Boschi-Pinto, C., Lopez, A., and Murray, C. (2002) Global and regional estimate of cancer mortality and incidence by site: II. Results for the global burden of disease 2000, *BMC Cancer 2*, 36−61.
10. Correia, J. J., and Lobert, S. (2001) Physicochemical aspects of tubulin-interacting antimitotic drugs, *Curr. Pharm. Des. 7*, 1213−1228.
11. Barbier, P., Gregoire, C., Devred, F., Sarrazin, M., and Peyrot, V. (2001) *In vitro* effect of Cryptophycin-52 on microtubule assembly and tubulin: Molecular modeling of the mechanism of action of a new antimitotic drug, *Biochemistry 40*, 13510−13519.
12. Nettles, J. H., Li, H., Cornett, B., Krahn, J. M., Snyder, J. P., and Downing, K. H. (2004) The binding mode of epothilone A on I,J-tubulin by electron crystallography, *Science 305*, 866−869.
13. Snyder, J. P., Nettles, J. H., Cornett, B., Downing, K. H., and Nogales, E. (2001) The binding conformation of Taxol in J-tubulin: A model based on electron crystallographic density, *Proc. Natl. Acad. Sci. U.S.A. 98*, 5312−5316.
14. Juménez-Barbero, J., Amat-Guerri, F., and Snyder, J. P. (2002) The solid state, solution and tubulin-bound conformations of agents that promote microtubule stabilization, *Curr. Med. Chem.: Anti-Cancer Agents 2*, 91−122.
15. Rai, S., and Wolff, J. (1996) Localization of the vinblastine-binding site on J-tubulin, *J. Biol. Chem. 271*, 14707−14711.
16. Mitra, A., and Sept, D. (2004) Localization of the antimitotic peptide and depsipeptide binding site on J-tubulin, *Biochemistry 43*, 13955−13962.
17. Bai, R. L., Petit, G. R., and Hamel, E. (1990) Binding of dolastatin 10 to tubulin at a distinct site for peptide antimitotic agents near the exchangeable nucleotide and Vinca alkaloid sites, *J. Biol. Chem. 265*, 17141−17149.
18. Loganzo, F., Discafani, C., Annable, T., Beyer, C., Musto, S., Hari, M., Tan, X., Hardy, C., Hernandez, R., Baxter, M., Singanallore, T., Khafizova, G., Poruchynsky, M. S., Fojo, T., Nieman, J. A., Ayral-Kaloustian, S., Zask, A., Andersen, R. J., and Greenberger, L. M. (2003) HTI-286, a synthetic analog of the tripeptide hemiasterlin, is a potent anti-microtubule agent that circumvents P-glycoprotein-mediated resistance *in vitro* and *in vivo*, *Cancer Res. 63*, 1838−1845.
19. Krishnamurthy, G., Cheng, W., Lo, M., Aulabaugh, A., Razinkov, V., Ding, W., Loganzo, F., Zask, A., and Ellestad, G. (2003) Biophysical characterization of the interactions of HTI-286 with tubulin heterodimer and microtubules, *Biochemistry 42*, 13484−13495.
20. Nunes, M., Kaplan, J., Wooters, J., Hari, M., Minnick, A. A., May, M. K., Shi, C., Musto, S., Beyer, C., Krishnamurthy, G., Qui, Y., Loganzo, F., Ayral-Kaloustian, S., Zask, A., and Greenberger, L. M. (2005) Two photoaffinity analogs of the tripeptide, hemiasterlin, exclusively label I-tubulin, *Biochemistry 44*, 6844−6857.
21. Zask, A., Birnberg, G., Cheung, K., Kaplan, J., Niu, C., Norton, E., Suayan, R., Yamashita, A., Cole, D., Tang, Z., Krishnamurthy, G., Williamson, R., Khafizova, G., Musto, S., Hernandez, R., Annable, T., Yang, X., Discafani, C., Beyer, C., Greenberger, L. M., Loganzo, F., and Ayral-Kaloustian, S. (2004) Synthesis and biological activity of analogs of the antimicrotubule agent $N,^{I},^{J}$-trimethyl-L-phenylalanyl-N^{1}-[(1*S*,2*E*)-3-carboxy-1-isopropylbut-2-enyl]-N^{1},3-dimethyl-L-valinamide (HTI-286), *J. Med. Chem. 47*, 4774−4786.
22. Zask, A., Birnberg, G., Cheung, K., Kaplan, J., Niu, C., Norton, E., Yamashita, A., Beyer, C., Krishnamurthy, G., Greenberger, L. M., Loganzo, F., and Ayral-Kaloustian, S. (2004) D-piece modifications of the hemiasterlin analog HTI-286 produce potent tubulin inhibitors, *Bioorg. Med. Chem. Lett. 14*, 4353−4358.
23. Niu, C., Smith, D., Zask, A., Loganzo, F., Discafani, C., Beyer, C., Greenberger, L. M., and Ayral-Kaloustian, S. (2004), Tubulin inhibitors. Synthesis and biological activity of HTI-286 analogs with B-segment heterosubstituents, *Bioorg. Med. Chem. Lett. 14*, 4329−4332.
24. Yamashita, A., Norton, E., Kaplan, J., Niu, C., Loganzo, F., Hernandez, R., Beyer, C., Annable, T., Musto, S., Discafani, C., Zask, A., and Ayral-Kaloustian, S. (2004) Synthesis and activity of novel analogs of hemiasterlin as inhibitors of tubulin polymerization: Modification of the A segment, *Bioorg. Med. Chem. Lett. 14*, 5317−5322.
25. Lowe, J., Li, H., Downing, K. H., Nogales, E. (2001) Refined structure of IJ-tubulin at 3.5 Å resolution, *J. Mol. Biol. 313*, 1045−1057.
26. *QUANTA*, Accelrys, Inc., San Diego, CA.
27. Nogales, E., Whittaker, M., Milligan, R., and Downing, K. (1999) High-resolution model of the microtubule, *Cell 96*, 79−88.
28. *Sybyl6.9*, Tripos, Inc., St. Louis, MO.
29. *OMEGA*, Open Eye Scientific Software, Santa Fe, NM.
30. *FRED*, Open Eye Scientific Software, Santa Fe, NM.
31. Verkivker, G. M., Bouzida, D., Gehlaar, D. K., Rejto, P. A., Arthurs, S., Colson, A. B., Freer, S. T., Larson, V., Luty, B. A., Marrone, T., and Rose, P. W. (2000) Deciphering common failures in molecular docking of ligand−protein complexes, *J. Comput.-Aided Mol. Des. 14*, 731−751.
32. Eldridge, M. D., Murray, C. W., Auton, T. R., Paolini, G. V., and Mee, R. P. (1997) Empirical scoring functions: I. The develop-

ment of a fast empirical scoring function to estimate the binding affinity of ligands in receptor complexes, *J. Comput.-Aided Mol. Des. 11*, 425−445.

33. Rush, T. S., Manas, E., Tawa, G., and Alvarez, J. (2005) Solvation-based scoring for high throughput docking, in *Virtual Screening in Drug Discovery* (Alvarez, J., and Shoichet, B., Eds.) pp 241−269, CRC Press, MA.
34. Ramnarayan, K., Chan, M. F., Balaji, V. N., Profeta, S., Jr., and Rao, S. N. (1995) Conformational studies on model dipeptides of Gly, L-Ala, and their C^{α}-substituted analogs, *Int. J. Pept. Protein Res. 45*, 366−376.
35. Poruchynsky, M. S., Kim, J. H., Nogales, E., Annabel, T., Loganzo, F., Greenberger, L. M., Sackett, D. L., and Fojo, T. (2004) Tumor cells resistant to a microtubule-depolymerizing hemiasterlin analog, HTI-286, have mutations in I- and J-tubulin and increased microtubule stability, *Biochemistry 43*, 13944−13954.
36. Gigant, B., Curmi, P. A., Martin-Brabey, C., Charbaut, E., Lachkar, S., Lebeau, S., Lebeau, L., Siavoshian, S., Sobel, A., and Knossow, M. (2000) The 4 Å X-ray structure of a tubulin: Stathmin-like domain complex, *Cell 102*, 809−816.

BI051268B